Journal of Hydrology 602 (2021) 126673

Contents lists available at ScienceDirect

Journal of Hydrology

journal homepage: www.elsevier.com/locate/jhydrol

Research papers

Comparison of soil dielectric mixing models for soil moisture retrieval using SMAP brightness temperature over croplands in India

Swati Suman [a], Prashant K. Srivastava [a,b,*], Dharmendra K. Pandey [c], Rajendra Prasad [d], RK Mall [b], Peggy O'Neill [e]

[a] Remote Sensing Laboratory, Institute of Environment and Sustainable Development, Banaras Hindu University, Varanasi 221005, India
[b] DST-Mahamana Centre for Excellence in Climate Change Research, Institute of Environment and Sustainable Development, Banaras Hindu University, Varanasi, India
[c] Space Applications Centre, Indian Space Research Organization, Ahmedabad, India
[d] Department of Physics, Indian Institute of Technology (BHU), Varanasi, India
[e] Hydrological Sciences Laboratory, NASA Goddard Space Flight Centre, Maryland USA

ARTICLE INFO

This manuscript was handled by Emmanouil Anagnostou, Editor-in-Chief, with the assistance of Viviana Maggioni, Associate Editor

Keywords:
Dielectric mixing models
Single Channel Algorithm
Soil Moisture Active Passive
Soil Moisture

ABSTRACT

The accurate estimation of soil moisture (SM) using microwave remote sensing depends mostly on careful selection of retrieval parameters among which the soil dielectric mixing model is the important one. These models are often categorized into empirical, semi-empirical or volumetric based on their methodologies and input data requirements. To study in detail, the comparative performance of four dielectric mixing models – Wang & Schmugge model, Hallikainen model, Dobson model and Mironov model were used with Soil Moisture Active Passive (SMAP) L-band brightness temperature and Single Channel Algorithm for SM retrieval over agricultural landscapes in India. The highest performance statistics combination in terms of Root Mean Square Error (RMSE), correlation coefficient (R^2) and percentage bias (PBIAS) against the concurrent in-situ SM measurements were calculated at the selected validation sites. The overall results indicate that the best performance was given by the Mironov model (RMSE = 0.07 m^3/m^3), followed by Wang & Schmugge model (RMSE = 0.08 m^3/m^3), Hallikainen model (RMSE = 0.09 m^3/m^3), Dobson model (RMSE = 0.10 m^3/m^3) and original SMAP radiometer SM (RMSE = 0.12 m^3/m^3). Findings of this study provides important insights into application and performance of dielectric mixing models in mapping surface SM variations. This study also underlines the pivotal role of local conditions for SM retrieval which should be carefully included in the algorithms.

1. Introduction

Soil Moisture (SM) is a significant component of the natural hydrological cycle. It was declared the "Essential Climate Variable" (ECV) in the year 2010 by the Global Climate Observing System. SM has extensive application in numerous hydro-meteorological studies including climate change, weather evolution, hydrological modelling and agricultural forecasting (Mladenova et al., 2011; Jackson, 1993). Due to its large spatial–temporal variations and the inability of point measurements for large scale spatial representation, it is very challenging to monitor SM at large spatial resolution using in-situ sensors (Al-Shrafany et al., 2012; Anav et al., 2018). However, Microwave Remote Sensing (MRS) techniques, both Active and Passive approaches have offered unique opportunities for global SM monitoring with their advantages and limitations.

The retrieval process using passive MRS depends mostly on the parameters involved such as dielectric mixing model, Land Surface Temperature (LST), Vegetation Water Content (VWC) etc. Among these parameters dielectric mixing model is a vital part of the retrieval process (Mironov et al., 2004). A dielectric constant is a complex number which represents the electrical property of the soil and is highly dependent on the moisture content at microwave frequencies. Several studies cites soil dielectric mixing models based on soil properties such as Wensink (1993), Knoll and Knight (1994), Heimovaara et al. (1994), Curtis (2001), Nguyen et al. (1997), Hallikainen et al. (1985), Wang and Schmugge (1980), Dobson et al. (1985), Mironov et al. (2004). These models are broadly categorized as 1. Phenomenological (Cole and Cole model (1941), Debye relaxation model (1929) 2. Volumetric (Complex Refractive Index, CRI model (1974); Maxwell De Loor model (1968)) 3. Empirical (Wang and Schmugge (1980)) 4. Semi-empirical (Dobson

* Corresponding author at: Remote Sensing Laboratory, Institute of Environment and Sustainable Development, Banaras Hindu University, Varanasi 221005, India.
E-mail address: prashant.iesd@bhu.ac.in (P.K. Srivastava).

https://doi.org/10.1016/j.jhydrol.2021.126673
Received 26 April 2021; Received in revised form 13 June 2021; Accepted 8 July 2021
Available online 13 July 2021

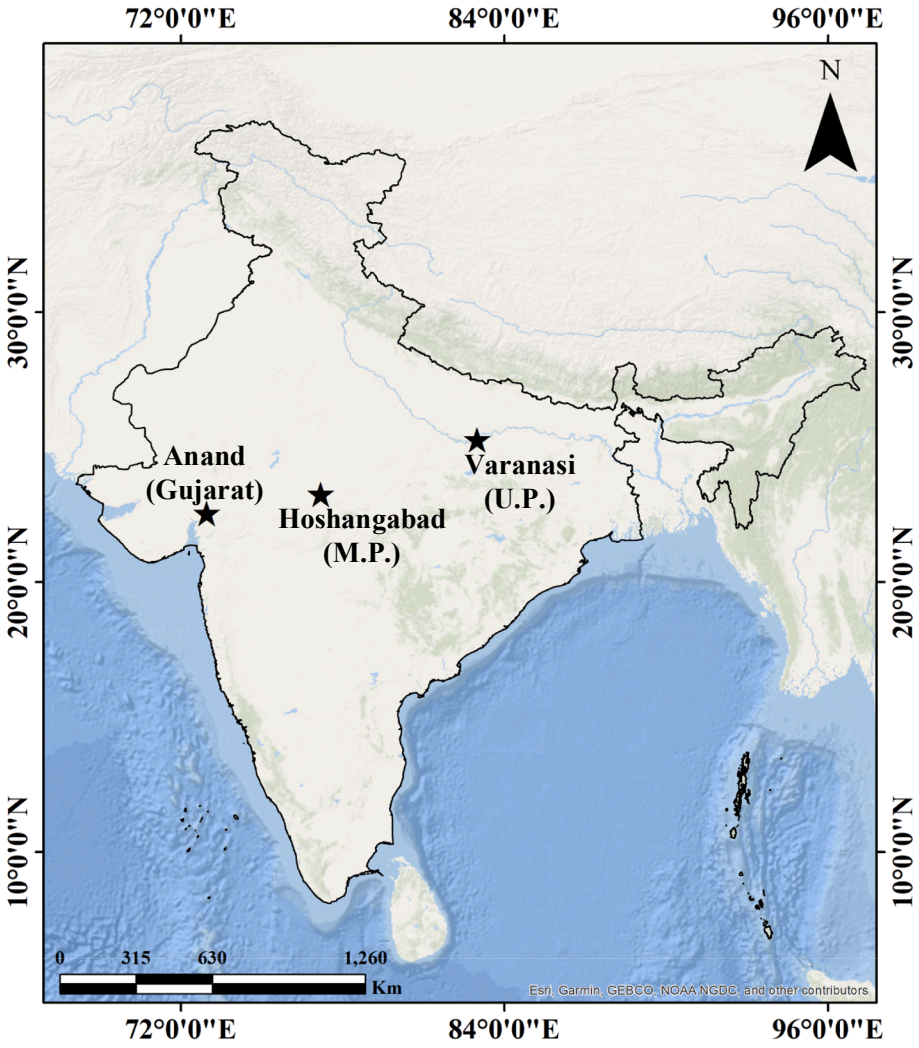

Fig. 1. Locations of the validation sites used in this study.

et al. model (1985), Mironov model) and 5. Volumetric based on the input data requirement (Srivastava et al., 2014; Van Dam, 2014; Van Dam et al., 2005). For passive-only L-band frequency-based SM retrieval approaches, dielectric models given by Mironov *et al.,* Dobson *et al.,* Wang &Schmugge *et al.,* and Hallikainen *et al.,* are reported to have the best performances due to their easy implementation and requirement of relatively fewer input parameters for calculation of various soil properties such as bulk density and sand and clay fractions compared to other models.

To retrieve SM using SMAP L1C brightness temperature product, Single Channel Algorithm (SCA) using Horizontal polarization is preferred in this study. SCA is an Inverse-based, single parameter model (Mladenova et al., 2014). The algorithm uses single frequency/polarization data, preferably the one sensitive to the SM (Jackson, 1993). SCA has a good heritage in SM retrieval under varying ground conditions in different climate regimes (Jackson, 1993; Jackson et al., 2002). The algorithm requires reliable ancillary data to estimate key parameters such as surface temperature, vegetation opacity, surface roughness and soil texture using local data which makes it most suitable for accurate SM retrieval at local scale than the global satellite SM products. SCA is also used as a baseline algorithm for developing SM products in SMAP mission and thus to present a comparative analysis on the performance of SMAP L3 radiometer product, developed on similar retrieval approach, the SCA algorithm was selected for this analysis as well. A detail description of the algorithm and a list various ancillary data and their sources is presented in the later section of this paper. Similarly, Microwave Polarization Difference Index (MPDI is also the most widely applied index used in the SM retrieval that links the effect of vegetation structure and cloud cover in the retrieval process (Felde, 1998). Variation in MPDI with the surface vegetation condition at all the selected sites is also discussed in detail in the Result section of this paper.

In this study, four state of the art soil dielectric mixing models were tested for Indian conditions where SM researches are often limited due to complex topographic features, extremely varying climatological and vegetation conditions and limited in-situ SM network. The four-soil dielectric mixing model most suitable for SM retrieval using passive microwave L-band brightness temperature are further explained in terms of the performances.

2. Study site and data set description

2.1. Study site characteristics

For this analysis, we selected three experimental sites located in India: Anand from Gujarat, Hoshangabad from Madhya Pradesh and Varanasi from Uttar Pradesh. These sites were selected mostly due to the easily accessible ground-based data set from the observational networks functioning at the selected locations. These in-situ SM data are believed to be crucial for validation of the output of this analysis. The characteristic of the ground measured SM measurement used in this analysis is

described in the following section of this paper. The first test site is situated in the Anand district of Gujarat. Anand is located in Gujarat's central region and covers a total area of 2941 square kilometers. According to the IMD climatological data, summers in Anand are extremely hot, and winters are cold. The region receives most of its rainfall during south west monsoon season during months of June to September with an annual rainfall record of 799.6 mm. Sandy loam and clay loam are the major soil types found in Anand. The second test site is situated in Hoshangabad, Madhya Pradesh located in India's central region. The winter season here begins in December and ends in February, with December being the coldest month with the lowest average minimum temperature followed by summer season starting from March to mid-June. The South West Monsoon occurs from June to September with an annual rainfall of 1225.9 mm. The major soil types found in Hoshangabad are black soils, ferruginous red lateritic soils, sandy clay loam, sandy loam and clay loam. The third test site is situated in the Varanasi, Uttar Pradesh. Varanasi's climate is sub-humid type, with hot summers, mild monsoons and moderate winters. The average annual rainfall is 1036.00 mm. The major soil types are sandy loam and clay loam. All the three test sites have uniform patches of crops around the sensor. Fig. 1 below shows the location of validation sites used in this analysis.

2.2. In-situ measurements

The in-situ SM data were obtained from the PAN India Network established by Space Applications Center (SAC) India Space Research Organization (ISRO) including daily measurement of SM and other physical and electrical properties of soil such as soil temperature and electric conductivity at different soil depths (0–5 cm, 5–10 cm, 10–15 cm) using Hydra probe sensors. Ground measured SM estimates at the selected validation sites, concurrent to SMAP overpass timings were preferred to be compared with retrieved SM data set using the selected dielectric models and SMAP radiometer SM product. Among the nine validation sites established across India by the ISRO's PAN India network, we selected the 03 locations having Hydra probe installed and continuous in-situ SM data are available to maintain data uniformity. TheHydra probe is a rugged SM sensor which operates at 50 MHz frequency. When this sensor is installed in soil, it evaluates the amplitude ratio of reflected waves within its probes and uses Maxwell's numerical equation to compute the real dielectric permittivity of the surrounding soil. The volumetric water content of the soil is then empirically correlated to the real dielectric permittivity. This method makes the probe immune to changes in soil texture, salinity, and temperature. The measurement zone of the sensor is 3 cm in diameter. The sensor's accuracy in all soil types is approx. 3% . The Hydra probe has also been used as a reliable instrument for measuring SM and other soil properties in different studies Chen et al., 2016, 2017; Colliander et al., 2017; Cosh et al., 2016; Wu and Margulis, 2013.

2.3. Satellite data description

2.3.1. SMAP L3 SM and LIC brightness temperature

The SMAP Level 3 Radiometer SM product (SPL3 SM P) provides global land surface SM estimates retrieved from the SMAP radiometer brightness temperature product. The product is then gridded and made available at 36 km EASE spatial resolution in HDF5 format to the users. This product is derived using Single Channel Algorithm (SCA) implemented on H-polarized brightness temperature (TB) data (Jackson et al., 2004). We selected this data product of SMAP due to its similar retrieval procedure which is also followed in this study other than its continuous availability over the validation sites. For this study, we processed the SMAP L3 SM data to get daily satellite SM estimates.

The Soil Moisture Active Passive (SMAP) L1C product is TB measurements of the earth surface at Vertical (V) and Horizontal (H) polarizations. The SMAP L1C product is also projected using a global grid based on the Equal-Area Scalable Earth (EASE) Grid at 36 Km in global projection, north projection and south projection. This product was used to extract daily TB over the selected validation site for SM retrieval using the SCA algorithm.

2.3.2. NASA global precipitation measurement Integrated Multi-SatellitE Retrievals for GPM (IMERG)

GPM mission is a world-wide network of satellites that offer global observations of rain and snow with a resolution of 0.1 degrees at every 30 min from 60^0N to 60^0S. It uses constellation of several multinational satellite missions such as GPM, Global Change Observation Mission-Water (GCOM-W1), National Oceanic and Atmospheric Administration (NOAA) space missions such as NOAA-18, MetOp series such Metop-A, and Metop-B to develop this product. To study the sensitivity of satellite and retrieved SM product in natural environment towards precipitation, global rainfall data set from the Global Precipitation Measurement Integrated Multi-satellitE Retrievals for GPM (IMERG GPM) were used in this study. Daily rainfall data set were downloaded from the website (https://pmm.nasa.gov/data-access/downloads/gpm). The data product has been very useful in recent studies such as Ma et al. (2019), Anjum et al. (2018), Carr et al. (2015) and Chen et al. (2016) to effectively assess the climatic, hydrological, and ecological conditions in different parts of the world by monitoring precipitation pattern over wide and complicated terrains.

2.3.3. Leaf Area Index (LAI), ERA-Interim LST product and FAO soil data set

The Copernicus Global Land Operation (CGLS) Leaf Area Index (LAI) Version 1 product has been used to estimate vegetation optical depth ($\boldsymbol{\tau}$) using Eq. (5), explained later in detail in the methodology section of this paper. The LAI product is provided as 30-day composite updated at every ten days. The LAI products were downloaded from the web portal (http://land.copernicus.eu/global/products). These data sets were processed using ArcGIS (Version 10.3) software.

ERA stands for the European Centre for Medium-Range Weather Forecasts (ECMWF) Re-Analysis and refers to the range of climate data sets produced as a result of series of research projects at ECMWF. The ECMWF skin temperature product was used to get daily Land Surface Temperature (LST) estimates used in this analysis. This data set refers to the radiometric temperature obtained from the thermal infrared spectrum.

Food and Agriculture Organization (FAO) provides global soil information with 30 arc-second resolution including top and subsoil property estimates for 15 different parameters including organic carbon, sand fraction, clay fraction, silt fraction, United States Department of Agriculture (USDA) soil texture, Reference Bulk Density, Soil Drainage property and soil phase information. The database was used to extract the Clay–sand fraction and bulk density for SM retrieval algorithm for the selected study sites using Arc GIS software (Version 10.1).

3. Methodology

3.1. Soil dielectric mixing models

This sub-section presents a small review of the widely used soil dielectric mixing models for L-band SM retrieval and used in this study viz. Wang &Schmugge model, Hallikainen model, Dobson model and Mironov model.

Wang &Schmugge model (1980) is an empirical dielectric mixing model that show effects of texture on the soil water dielectric constant. This model was developed using the variation of soil dielectric characteristics as a function of soil moisture content in various soil types and used the known dielectric constants or refraction indices of air, water, and ice, as well as the volume percent of each ingredient, to compute the dielectric constant of the soil. Hallikainen et al.,(1985) dielectric model is an empirical mixing model that estimates the dielectric constant of soil -water mixture more precisely and accurately over frequency 1–18 GHz

Table 1
Ancillary Data and sources used in this study.

Parameters	Description/Data Sources
Soil Temperature	European Centre for Medium Range Weather Research Forecast (ECMWF) Forecast Temperature
Vegetation Water Content (VWC)	European Space Agency (ESA) Copernicus Global Land Operation (CGLS) Leaf Area Index (LAI)
Sand and Clay Fraction	Food and Agriculture Organisation (FAO) Harmonized World Soil Data set (HWSD)
Precipitation	NASA Global Precipitation Measurement Integrated Multi-SatellitE Retrievals for Global Precipitation Mission (GPM) (IMERG)
Land Cover Class	Moderate Resolution imaging Spectroradiometer (MODIS) International Geosphere-Biosphere Program (IGBP) Combined Land Cover Product

for different soil types based on specified soil physical characteristics. The microwave dielectric constant of the soil in this model is represented as functions of SM content, physical temperature and soil texture. Dobson et al. model (1985) is a semi-empirical dielectric mixing model based on the refractive index requiring readily available soil physical parameter's information such as volumetric SM content (m_v), bulk density (ρ_b) and percentage of sand (S) and clay (C) fraction. Mironov Mixing model is a generalized refractive dielectric mixing model (GRMDM) suitable for a comprehensive range SM, soil type and frequency (Mironov et al., 2004). This model introduced the concept of the intrinsic bound soil water (BSF) and free-soil water (FSW) and the complex dielectric constant (CDC) fitting method. A detail description of the above-mentioned dielectric models by the authors in this paper with their working formulas and studies citing their application has been recently published in Soil Moisture Product Validation, Best Practice Protocol released by NASA (Montzka et al., 2020)

3.2. Single Channel Algorithm for SM retrieval

For correction of vegetation parameters such as Vegetation Water Content (VWC), the SCA algorithm uses ancillary information such as Normalized Difference Vegetation Index (NDVI) or Leaf Area Index (LAI), and other data such as Land cover, LST, Soil information. Table 1 enlists all the ancillary data and their source for SM retrieval used in this analysis. SCA assumes the single scattering albedo, $\omega = 0$ and minimal atmospheric contribution. The expression for TB is presented as

$$TB_{(f,p)} = T_s\left\{1 - \left(1 - e_{s,rough}\right)\left(e^{\left[\frac{-\tau}{\cos\theta}\right]}\right)^2\right\} \quad (1)$$

where TB = brightness temperature, p = polarization, T_s = surface physical temperature, $e_{s,rough}$ = rough surface emissivity, τ = vegetation optical depth and θ = angel of incidence.

Considering all assumptions, reflectivity equation for smooth surface can be presented as

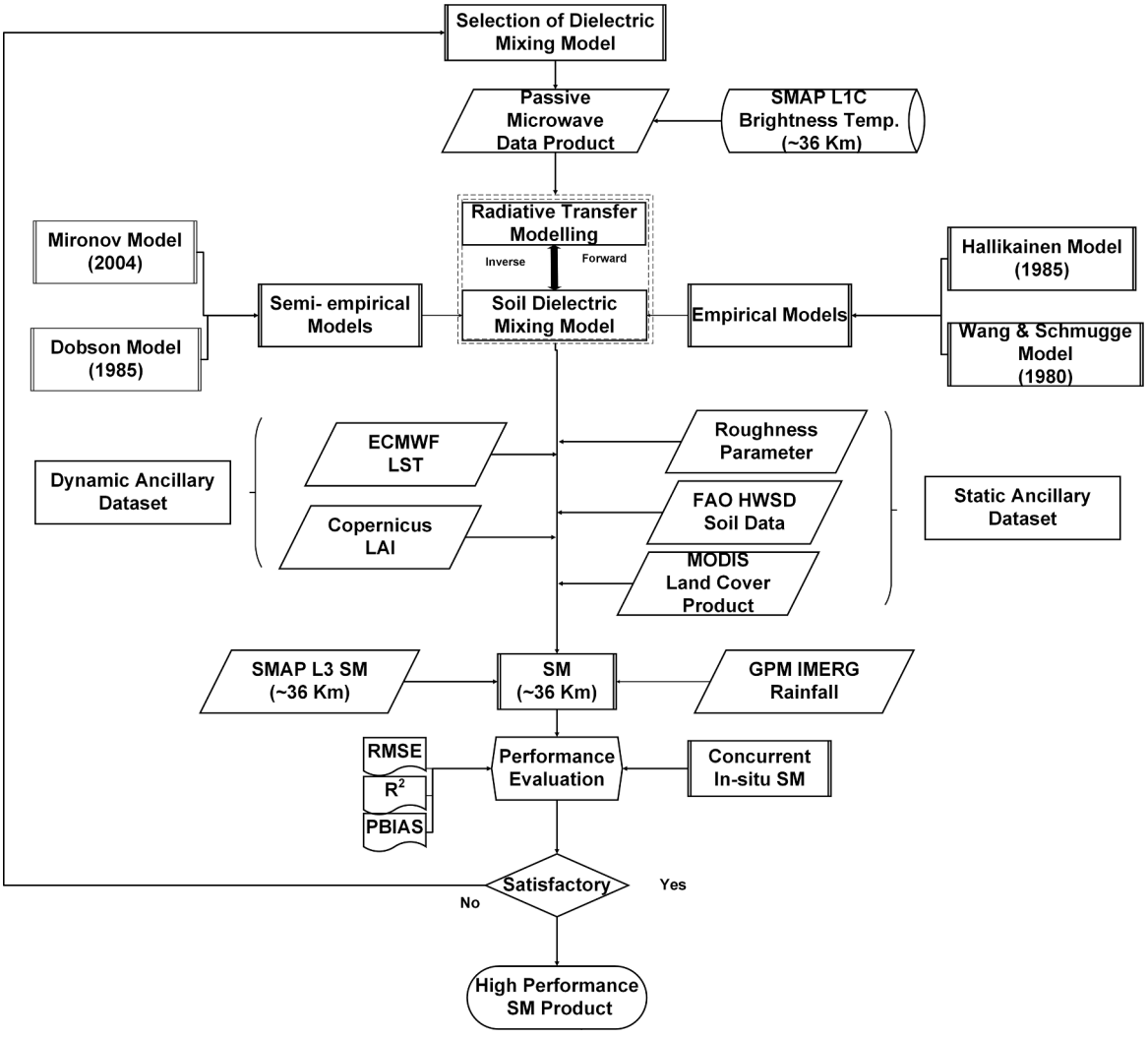

Fig. 2. Methodology followed in this study.

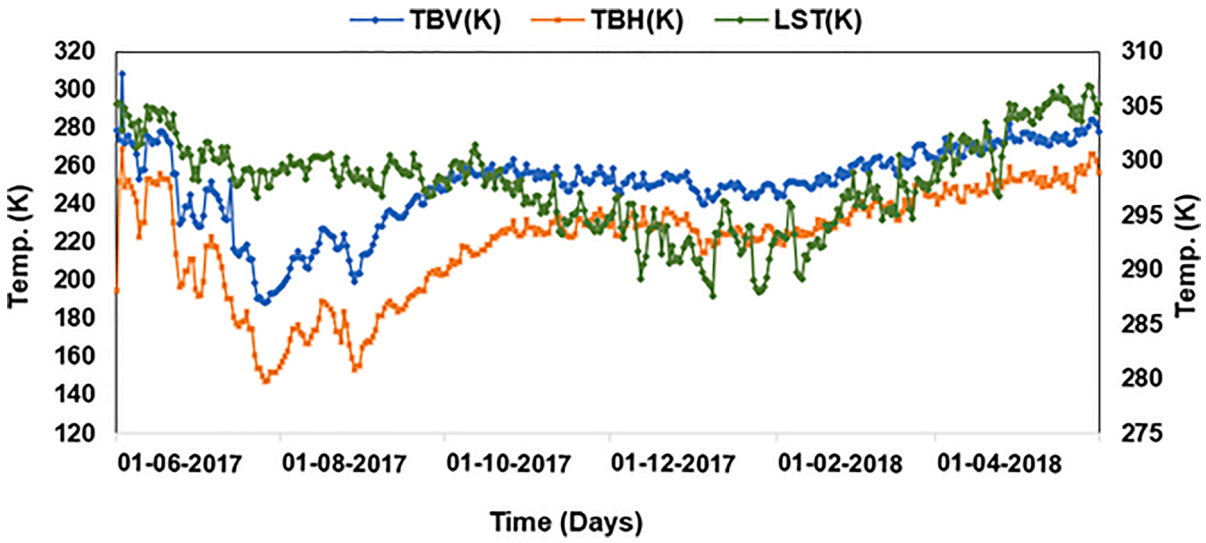

Fig. 3. Graph showing variation in TBV, TBH (using primary Y-axis on the left side) and LST (using secondary Y-axis on the right side) over the entire study period for Anand, Gujarat.

$$R_{(f,p)}^{smooth} = \left\{ \left(1 - \left(\frac{TB_{(f,p)}}{T_s}\right)\right) e^{\left[h\cos^2\theta + 2b * \frac{VWC}{\cos\theta}\right]} \right\} \quad (2)$$

In the above equation $R_{(f,p)}^{s,smooth}$ = smooth surface reflectivity, T_s = surface temperature, VWC = Vegetation Water Content, θ = angel of incidence.

The SCA-H model requires soil texture and land use/land cover patterns which were obtained using gravimetric methods, soil cover maps and on-site inspections.

Tau-omega (τ − ω) is considered as the approximate form of radiative transfer equation , which is based on two parameters, the vegetation optical depth, τ and the vegetation scattering albedo, ω. These two variables are used to parametrize the vegetation attenuation properties and the scattering effects. Low vegetation, τ − ω model is expressed as

$$TB_p = (1-\omega)\left(1-\gamma_p\right)\left(1+\gamma_p r_{gp}\right)T_c + \left(1-r_{gp}\right)\gamma_p T_g \quad (3)$$

where T_g and T_c are the effective soil and vegetation temperatures, p represents particlular polarization, r_{gp} is the soil reflectivity, ω_p is the single scattering albedo, γ_p is the vegetation attenuation factor; derived from the τ_p using the formula

$$\gamma_p = exp\left(-\tau_p/cos\theta\right) \quad (4)$$

where the optical depth, τ_p is calculated using formula

$$\tau_p = b_p * VWC \quad (5)$$

where b_p is the crop factor (Jackson and Schmugge, 1991).

For the surface temperature, it is assumed that the effective soil (T_g) and vegetation temperature (T_c) are approximately equal to a single value

$$T_{gc} \approx T_c \approx T_g \quad (6)$$

where T_{gc} is the surface temperature including both soil and vegetation and is derived using the formula

$$T_{gc} = A_t T_c + (1 - A_t)\, T_g \quad (7)$$

where, $A_t = B_t(1 - exp(\tau_{NAD}))$, τ_{NAD} is VOD at the nadir point.

The methodology followed in this analysis is shown in Fig. 2. In summary, we applied the above-mentioned soil dielectric mixing models with the SCA algorithm using the SMAP L1C TB product to retrieve surface SM estimates at the chosen validation sites located around vast uniform patches of agricultural land and analyzed their performance with in-situ data using performance statistics to obtain high performance SM product. Also, to study the sensitivity of the satellite and retrieved SM products in natural environment, we used high resolution NASA GPM IMERG precipitation data and studied their behavior over the time period of this study.

3.3. Performance statistics

To assess the performance of the dielectric models used in this study we used 3 performance statistics widely used to compare the model performance such as Root Mean Square Error (RMSE), Square of Correlation (R^2) and Percentage Bias (PBIAS). Based on the results , performance of these models for each site is presented in detail .

The RMSE estimates the standard deviation of the model prediction error and measures the average magnitude of the error. A small RMSE value indicates better model performance whereas a higher value indicates a poor performance of the model. The formula for calculating RMSE is shown as

$$RMSE = \sqrt{\sum_{i=1}^{N} \frac{(y_i - x_i)^2}{N}} \quad (8)$$

where, x and y are the observed and simulated data set respectively and N is total number of observations.

Square of Correlation (R^2) represents the strength of the linear association between two variables and its value ranges between −1 and 1 representing a prefect a negative and positive correlation respectively. Values near to 1 represents strong correlation. The formula for calculating correlation can be represented as

$$R^2 = 1 - \frac{\sum_{i=1}^{N} [y_i - x_i]^2}{\sum_{i=1}^{N} [x_i - \bar{x}_i]^2} \quad (9)$$

where, x and y are the observed and simulated data set respectively, N is the total number of observations and $\bar{x}$ is the mean of x.

The PBIAS is used to estimate the average bias in the simulated values and its optimal value is 0.0 which indicates the ideal model simulation. PBIAS value greater than 0 represents an overestimation whereas lesser value indicates an underestimation bias. The equation for PBIAS is written as

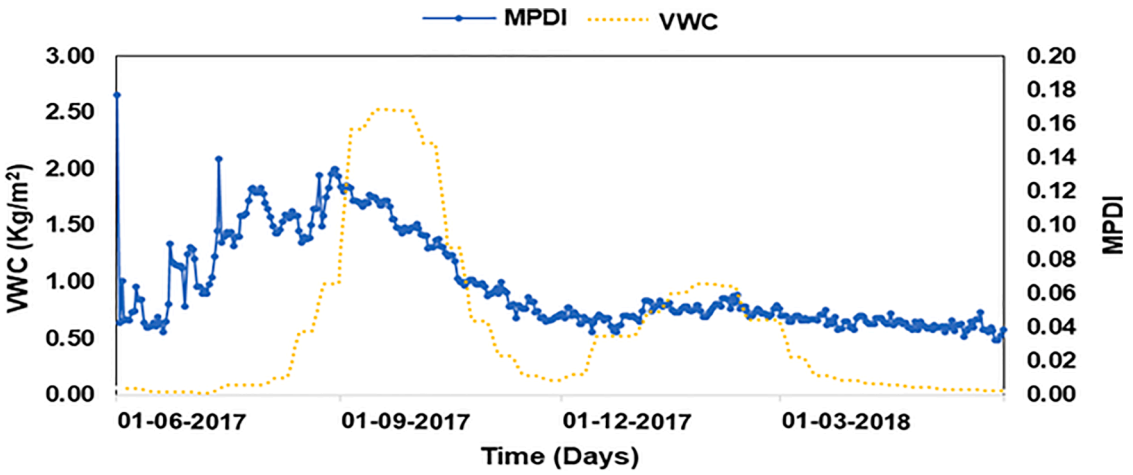

Fig. 4. Graph showing variation in VWC and MPDI over the entire study period for Anand, Gujarat.

$$PBIAS = 100^{*}\frac{\sum_{i=1}^{N}(y_i - x_i)}{\sum_{i=1}^{N}x_i} \quad (10)$$

where, x and y are the observed and simulated data set respectively and N is the total number of observations.

4. Result and discussion

In this section, a detailed description about the behavior of SM retrieval parameters– LST, TB, LAI, MPDI and performance of the SM retrieval algorithm in estimating SM for each experimental site is presented.

For studying the seasonal variation in the retrieval parameters , especially for the LST and TB, we selected the four seasons defined by the Indian Meteorological Department (IMD), Government of India; Winter (December–February), Summer (March–May), Monsoon (June–September) and Post-Monsoon (October–November). Also, to understand the variation in the vegetation parameters – VWC and MPDI , we considered the two cropping seasons used for agriculture in India i. e. Kharif or Monsoon crops (July–October) and Rabi or winter crops (October–March) (Indian Meteorological Department; IMD, Government of India).

4.1. Anand, Gujarat

4.1.1. Temporal behavior of TB and SM retrieval parameters at the station

Anand has a tropical type of climate where average temperature rises at peak during months of April – May and precipitation here is influenced by the monsoon climate of India. To study the variation in LST and TB at H-polarization (TBH) and V-polarization (TBV), we used a temporal plot as shown in Fig. 3.The average LST during the whole study period (June 2017–May 2018) was reported to be around 298 K and not

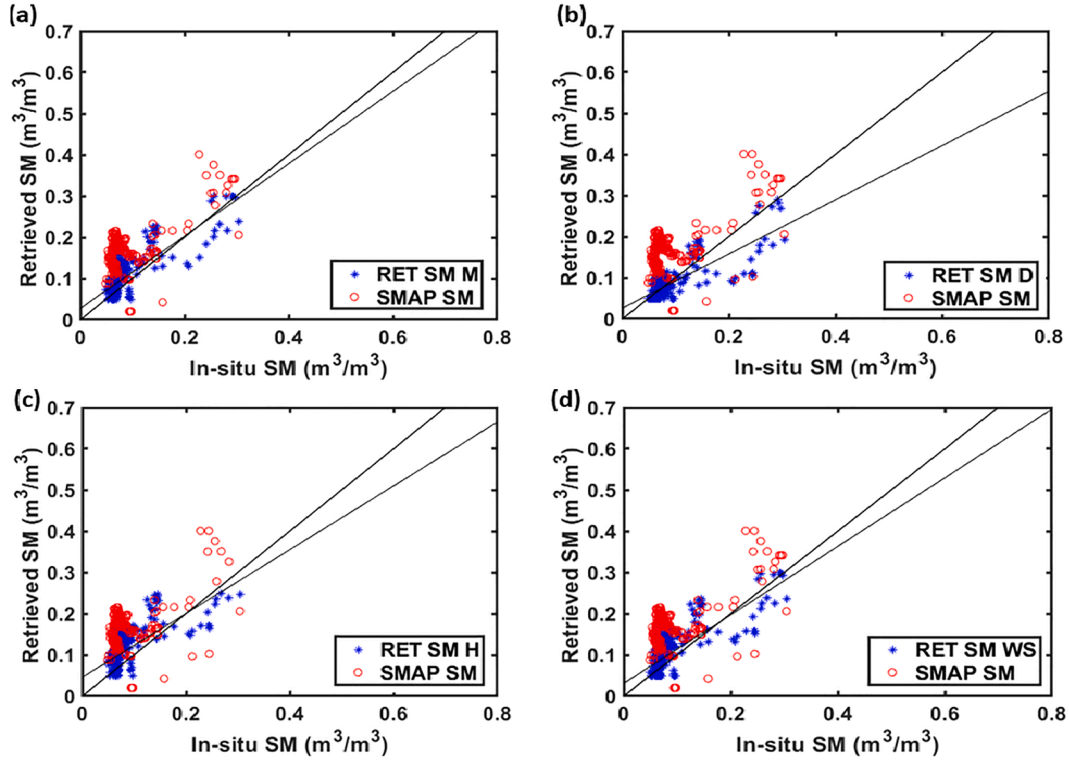

Fig. 5. Scatterplot between In-situ, SMAP SM, GPM rainfall at the Anand, Gujarat for (a) RET SM M, (b) RET SM D, (c) RET SM H, (d) RET SM WS.

Table 2
Results of comparison of different Dielectric Models used in this study at Anand Gujarat, India.

Statistical test	SMAP SM	Mironov	Dobson	Hallikainen	Wang & Schmugge
Square of Correlation (R^2)	0.34	0.68	0.63	0.51	0.61
RMSE (m^3/m^3)	0.09	0.03	0.03	0.04	0.04
PBIAS	43.60	5.0	−5.40	12.0	4.80

much variation can be noticed unlike the TBV (av. = 250 K) and TBH (av. = 221 K) where a significant decrease was noted during monsoon season (July–September) was observed.

From Fig. 4 an increasing trend in VWC can be noticed during the starting phase of the study period, during June–July 2017 and reaching its maximum value during August–September could be related to sowing, growing and maturing phases of the Kharif crops such as rice millet and groundnuts predominantly grown in the regions. A decreasing trend was observed during October–November may be due to harvesting of the crops. Again, an increasing trend can be observed in VWC during winter months i.e. January–February 2018, due to growth of Rabi crops (Wheat, barley and cereals), decreasing post-March indicating harvesting of the Rabi crops and end of the agricultural year at the site. MPDI can also be noticed increasing during June–-August 2017 and reaching at its maximum during September with high SM content during monsoon and low VWC during early growing stage of crops. A constant trend postMarch indicating harvesting of the Rabi crops and end of the agricultural year at the site.

4.1.2. Performance comparison at the Anand station

At Anand, Mironov model (RMSE = 0.03, R^2 = 0.68, PBIAS = 5.0) performed best in retrieving SM estimates than Dobson model (RMSE = 0.03, R^2 = 0.63, PBIAS = −5.40), Wang &Schmugge (RMSE = 0.04, R^2 = 0.61, PBIAS = 4.80) and Hallikainen model (RMSE = 0.04, R^2 = 0.51, PBIAS = 12.0). All the models performed better than the SMAP SM (RMSE = 0.09, R^2 = 0.34, PBIAS = 43.60) when compared against the in-situ SM values and in mapping surface SM changes at the site. PBIAS results showed an overestimation by Wang &Schmugge model (PBIAS = 4.80), Mironov model (PBIAS = 5.0), Hallikainen model (PBIAS = 12.0) and SMAP SM (PBIAS = 43.60) while an underestimation by Dobson model (PBIAS = −5.40). Scatter plot between the in-situ SM, SMAP SM, retrieved SM using Mironov dielectric model (RET SM M) is presented in Fig. 5 (a) along with retrieved SM using Dobson dielectric model (RET SM D) in Fig. 5(b), retrieved SM using Hallikainen dielectric model (RET SM H) in Fig. 5(c), retrieved SM using Wang & Schmugge dielectric model (RET SM WS) in Fig. 5(d). Results of the performance analysis is shown in Table 2.

4.1.3. Temporal consistency at the station

For Anand, Fig. 6 (a) presents the temporal series plot between in-situ SM, Mironov retrieved SM (RET SM M), SMAP SM and GPM rainfall and Fig. 6(b) for Dobson model retrieved SM (RET SM D) over Anand between June 2017–May 2018. Heavy rainfall can be seen during July–September 2017 and also few days of significant downpour during January and February 2018. During these days in-situ SM reached at its maximum values due rainfall and resulting increased SM content. SMAP SM can be seen overestimating the in-situ SM but responding well to the sudden moisture change at the site. During the entire study period, RET SM M overestimated the in-situ SM but can be seen in close approximation to the observed SM compared to the SMAP SM. A gap in the

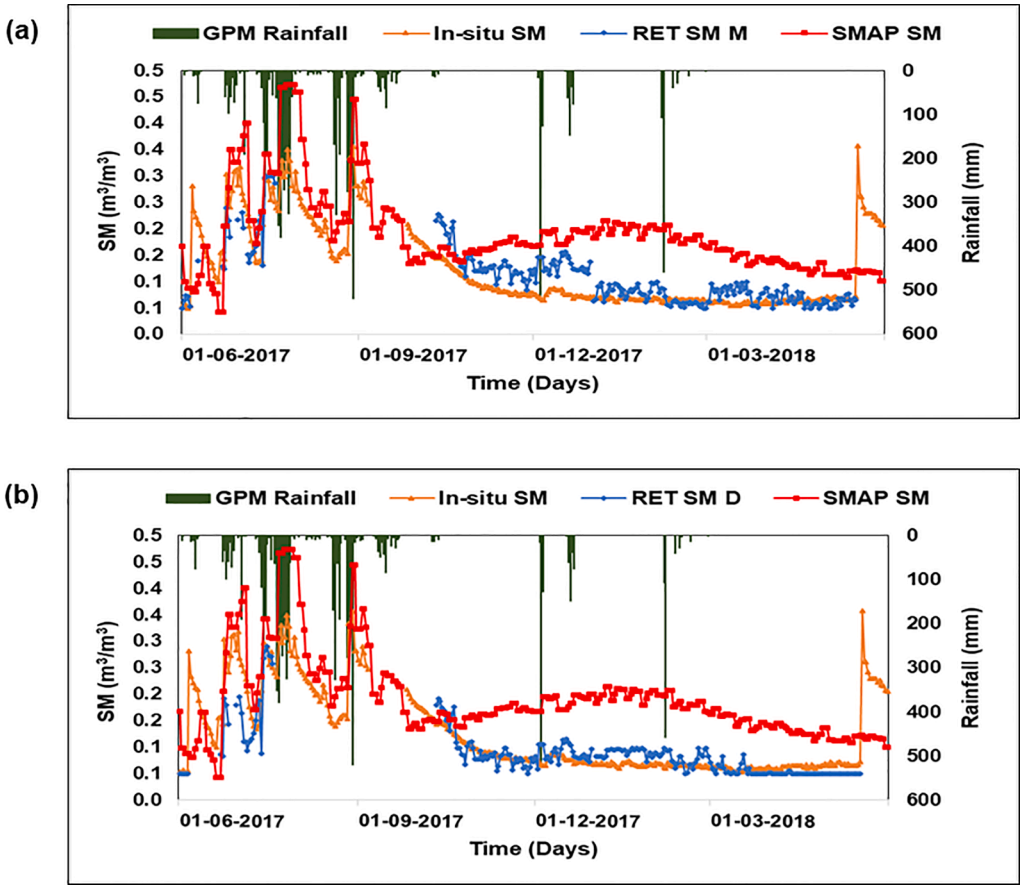

Fig. 6. Temporal plot between In-situ, SMAP SM, GPM rainfall at the Anand, Gujarat for (a) RET SM M, (b) RET SM D.

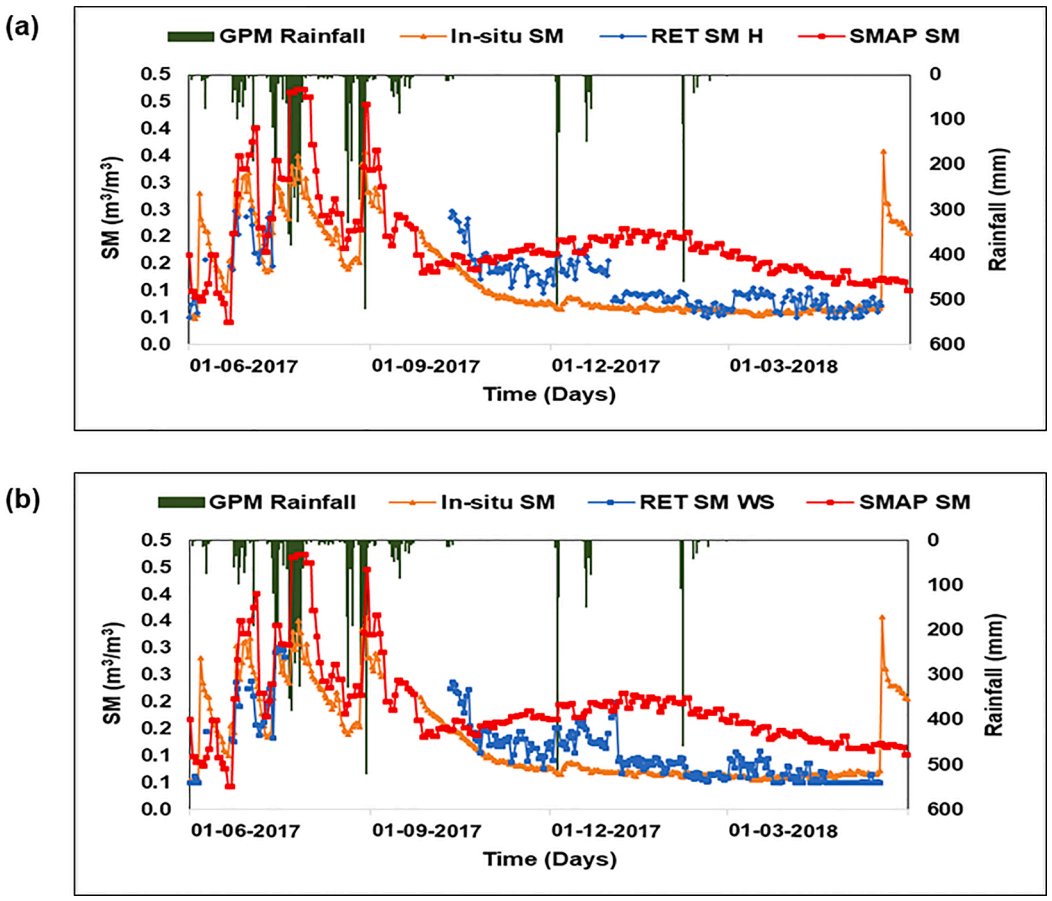

Fig. 7. Temporal plot between In-situ, SMAP SM, GPM rainfall at the Anand, Gujarat for (a) RET SM H, (b) RET SM W.

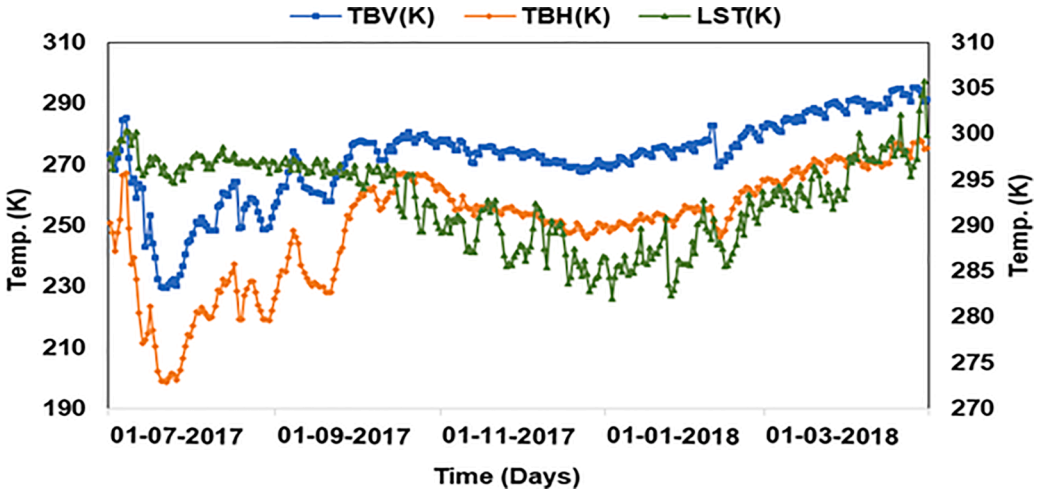

Fig. 8. Graph showing variation in TBV,TBH (using primary Y-axis on the left side) and LST (using secondary Y-axis on the right side) over the entire study period for Hoshangabad, M.P.

retrieved SM can be observed during the days of heavy rainfall due to limitation of these models in capturing this sudden change on local environment and extreme weather conditions resulting repeated value at the upper value of SM range considered for the analysis. In Fig. 6(b) Dobson retrieved SM (RET SM D) can also be seen producing SM estimates close to the in-situ SM but can also be noticed to be underestimating the observed SM during some days in July November, December 2017 and at the last phase of the study period; March–May 2018 showing a saturated value to the lower limit considered for the simulation.

Fig. 7(a) and (b) shows the daily performance of the Hallikainen retrieved SM (RET SM H) and Wang &Schmugge retrieved SM (RET SM W) with in-situ SM, SMAP SM and its response to the precipitation represented by the GPM rainfall respectively. The Hallikainen retrieved SM overestimated the in-situ SM for a significant period from August 2017 to February 2018 and during the few days of March and April 2018. Wang &Schmugge model also overestimated the ground measured SM during August 2017 to February 2018 and few days during

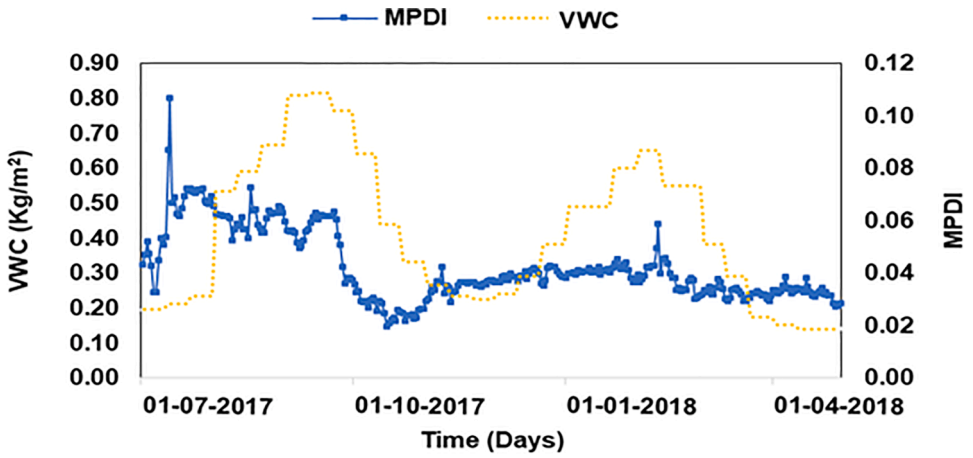

Fig. 9. Graph showing variation in VWC and MPDI over the entire study period for Hoshangabad, M.P.

Table 3
Results of comparison of different Dielectric Models used in this study at Hoshangabad, M.P., India.

Statistical test	SMAP SM	Mironov	Dobson	Hallikainen	Wang & Schmugge
Square of Correlation (R^2)	0.84	0.70	0.76	0.74	0.78
RMSE (m^3/m^3)	0.13	0.10	0.13	0.11	0.10
PBIAS	−28.10	−18.10	−26.10	−22.50	−18.70

March 2018 and then limited to the lowest SM limit during April–May 2018. At Anand, Mironov and Hallikainen models were more efficient in mapping SM variation under natural condition than Dobson and Wang & Schmugge .

4.2. Hoshangabad, Madhya Pradesh

4.2.1. Temporal behavior of TB and SM retrieval parameters at the Hoshangabad station

The temporal plot between TBV, TBH and LST for the Hoshangabad is shown in Fig. 8. The average LST from July 2017 to April 2018 was 298 K whereas for TBV was 267 K and TBH was 243 K. TB could be noticed lowest from June to September 2017 probably due to rainfall during monsoon season. Temperature was marked gradually increasing

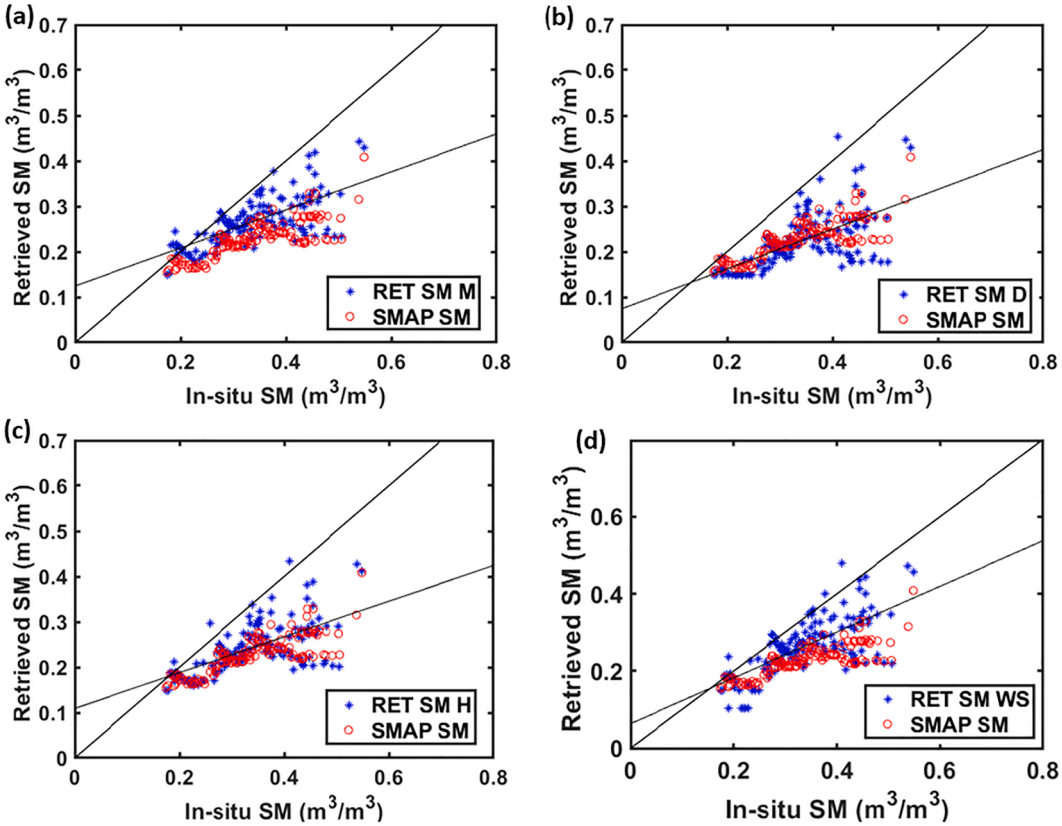

Fig. 10. Scatterplot between In-situ, SMAP SM, GPM rainfall at the Hoshangabad, M.P. for (a) RET SM M, (b) RET SM D, (c) RET SM H, (d) RET SM WS.

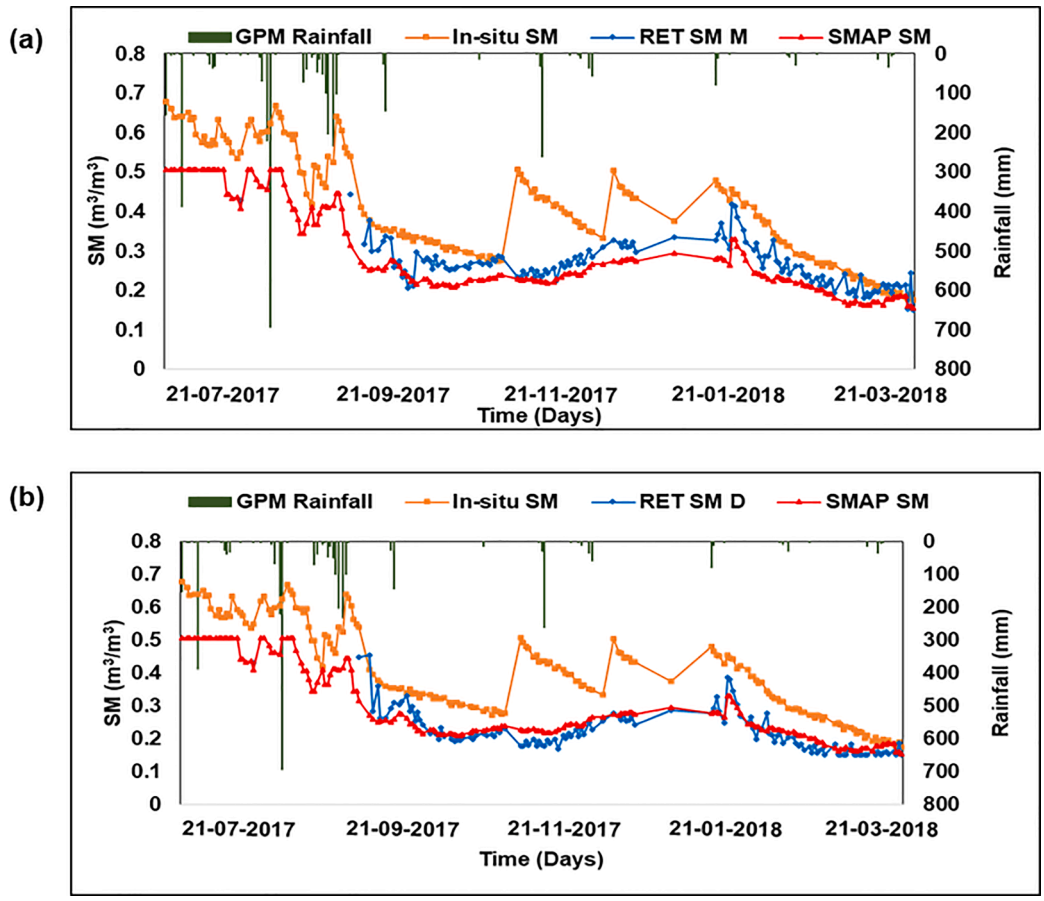

Fig. 11. Temporal plot between In-situ, SMAP SM, GPM rainfall at the Hoshangabad, M.P for (a) RET SM M, (b) RET SM D.

and getting its peak during April 2018 due to summer season.

Fig. 9 presents temporal variation in VWC and MPDI over Hoshangabad. VWC can be seen gradually increasing during sowing and growth stages for both the seasons (Kharif during July-September and Rabi crops during November 2017–January 2018), highest VWC is evident at their mature stage i.e. between September 2017 and February 2018 respectively. Low values can be noticed during the end of both the cropping seasons indicating harvesting of the crops. MPDI was recorded highest during starting stage and prevailing monsoon at the site while gradually decreasing with the increase in VWC during the rest of the time period.

4.2.2. Performance comparison at the station

Results of the statistical tests show the best performance by Mironov (RMSE = 0.10) and Wang & Schmugge model (RMSE = 0.10) with less error compared to Hallikainen model (RMSE = 0.11) and Dobson model (RMSE = 0.13) but based on the correlation between the retrieved SM and in-situ SM; Wang &Schmugge model ($R^2 = 0.78$) performed slightly better than Dobson model ($R^2 = 0.76$,) followed by Hallikainen model ($R^2 = 0.74$) and Mironov model ($R^2 = 0.70$). SMAP SM (RMSE = 0.13, $R^2 = 0.84$, PBIAS = −28.10) marginally performed better in retrieving the SM estimates at the site compared all other models. Interestingly all models as well satellite SM showed an underestimating pattern in retrieval; Mironov model (PBIAS = −18.10), Wang & Schmugge model (PBIAS = −18.70), Hallikainen model (PBIAS = −22.50), Dobson model (PBIAS = −26.10), when compared with the in-situ measured values. Results are presented in Table 3 while the scatter plots between the data sets; in-situ SM, SMAP SM retrieved SM using Mironov dielectric model (RET SM M) is presented in Fig. 10(a) along with retrieved SM using Dobson dielectric model (RET SM D) in Fig. 10(b), retrieved SM using Hallikainen dielectric model (RET SM H) in Fig. 10(c), retrieved SM using Wang & Schmugge dielectric model (RET SM WS) in Fig. 10(d).

4.2.3. Temporal consistency at the station

Fig. 11(a) and (b) show the temporal performance of Mironov and Dobson dielectric models in SM retrieval compared to in-situ SM, SMAP SM and GPM rainfall during July 2017 to April 2018 over Hoshangabad, M.P. For the entire span of this study, all-dielectric models retrieved SM estimates and SMAP SM show underestimated SM measurements. Still, Mironov retrieved SM (RET SM M) performed better, whereas Dobson retrieved SM (RET SM) showed a similar pattern as SMAP SM. A closer approximation between Mironov SM and in-situ SM values can be noticed during January–April 2018. Significant of rainfall can be seen during July–September 2017 and also during November, January and March months.

Hallikainen and Wang & Schmugge also performed well at Hoshangabad in mapping surface SM variation. Hallikainen derived SM estimate had a similar variation trend as SMAP SM. In contrast, Wang & Schmugge model performed better than SMAP SM and retrieved SM estimates can be noticed closer to the in-situ SM estimates during the entire study period. The temporal plot for Hallikainen retrieved SM with in-situ SM, SMAP SM, and GPM rainfall is shown in Fig. 12(a) and for Hallikainen and Wang & Schmugge model in Fig. 12(b) respectively.

4.3. Varanasi, Uttar Pradesh

4.3.1. Temporal behavior of TB and SM retrieval parameters at the Varanasi station

The average TBV recorded at Varanasi was 268 K whereas for TBH it was 233 K and LST 300 K during June 2017–May 2018. LST at the site looks uniform except a slight decrease during winter months, December 2017–March 2018. A decreasing trend in TBV and TBH was noticed

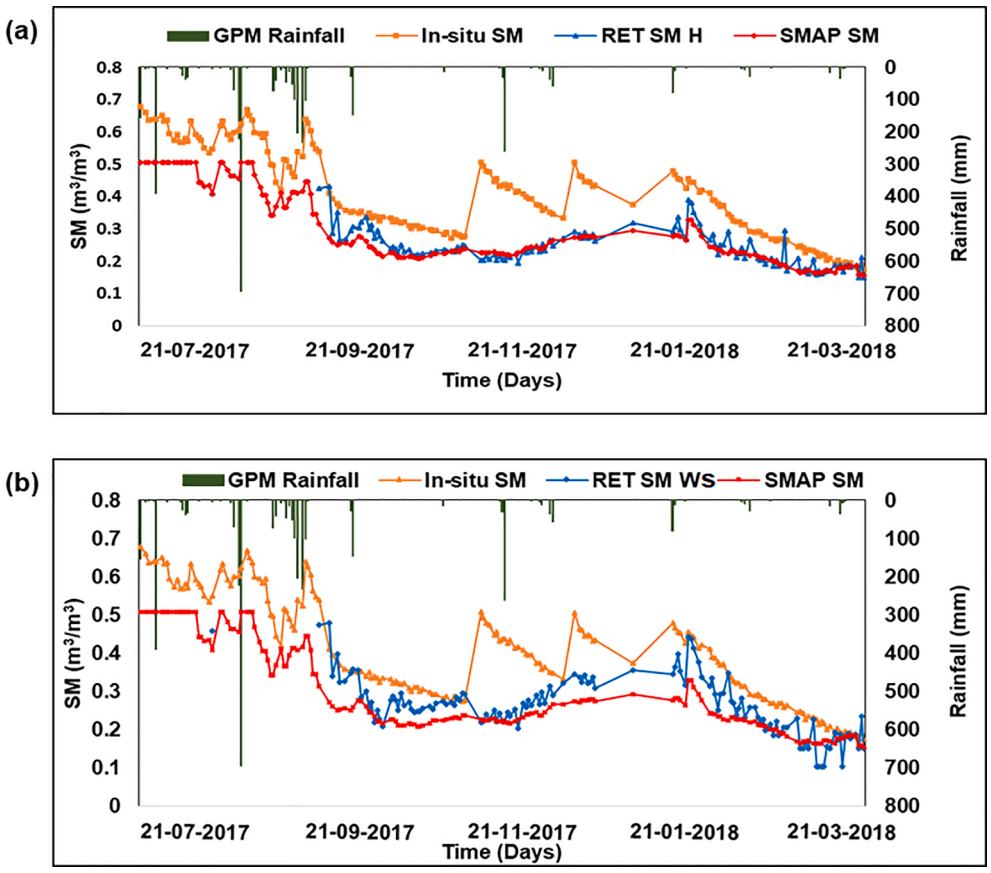

Fig. 12. Temporal plot between In-situ, SMAP SM, GPM rainfall at the Hoshangabad, M.P for (a) RET SM H, (b) RET SM W.

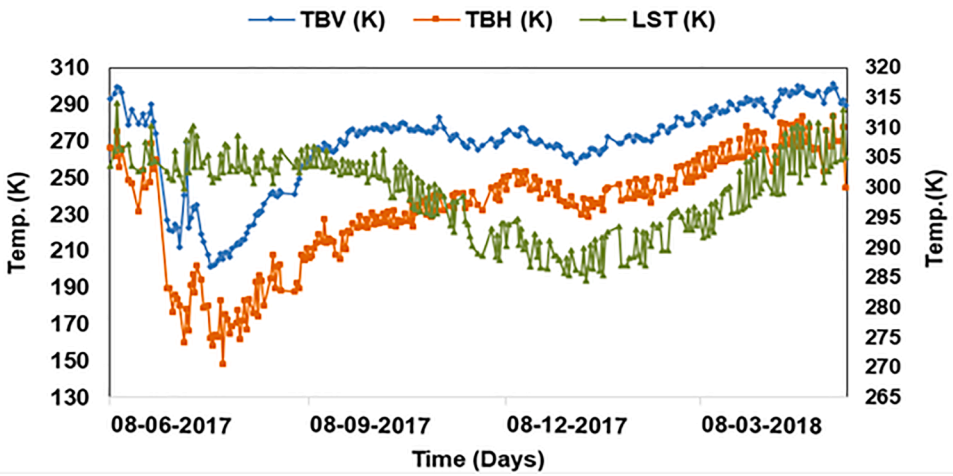

Fig. 13. Graph showing variation in TBV,TBH (using primary Y-axis on the left side) and LST (using secondary Y-axis on the right side) over the entire study period for Varanasi, UP.

during the monsoon and winter months. The temporal plot between TBV, TBH and LST for Varanasi site is presented in Fig. 13.

VWC can be noticed increasing during June and reaching at its peak during July–September 2017 due to maturing of the Kharif crops at the site and slowly decreasing during October–November 2017 with the harvesting of the crop's indicating less agricultural activities at the site. An increasing VWC can be noted again during December 2017 and reaching its peak during December 2017–February 2018. MPDI can also be seen as varying in a similar pattern with VWC. An increasing trend in MPDI can be seen with the sowing and growth of crops and maximum during its mature stage in the both the cropping seasons. A temporal plot between VWC and MPDI for the Varanasi is presented in Fig. 14.

4.3.2. Performance comparison at the station

At Varanasi, Mironov model (RMSE = 0.08, R^2 = 0.82, PBIAS = −19.60) performed better than Wang & Schmugge (RMSE = 0.09, R^2 = 0.81, PBIAS = −23.20), Hallikainen model (RMSE = 0.10, R^2 = 0.79, PBIAS = −26.40) and Dobson model (RMSE = 0.11, R^2 = 0.79, PBIAS = −29.80). PBIAS results showed an underestimation by the retrieved and satellite SM data sets compared to the in-situ data estimates. SMAP SM

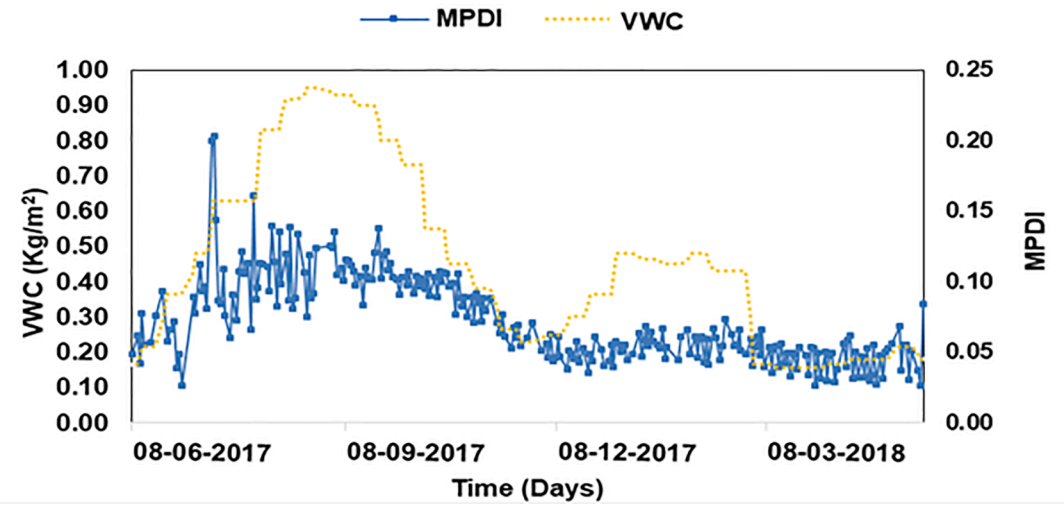

Fig. 14. Graph showing variation in VWC and MPDI over the entire study period for Varanasi, UP.

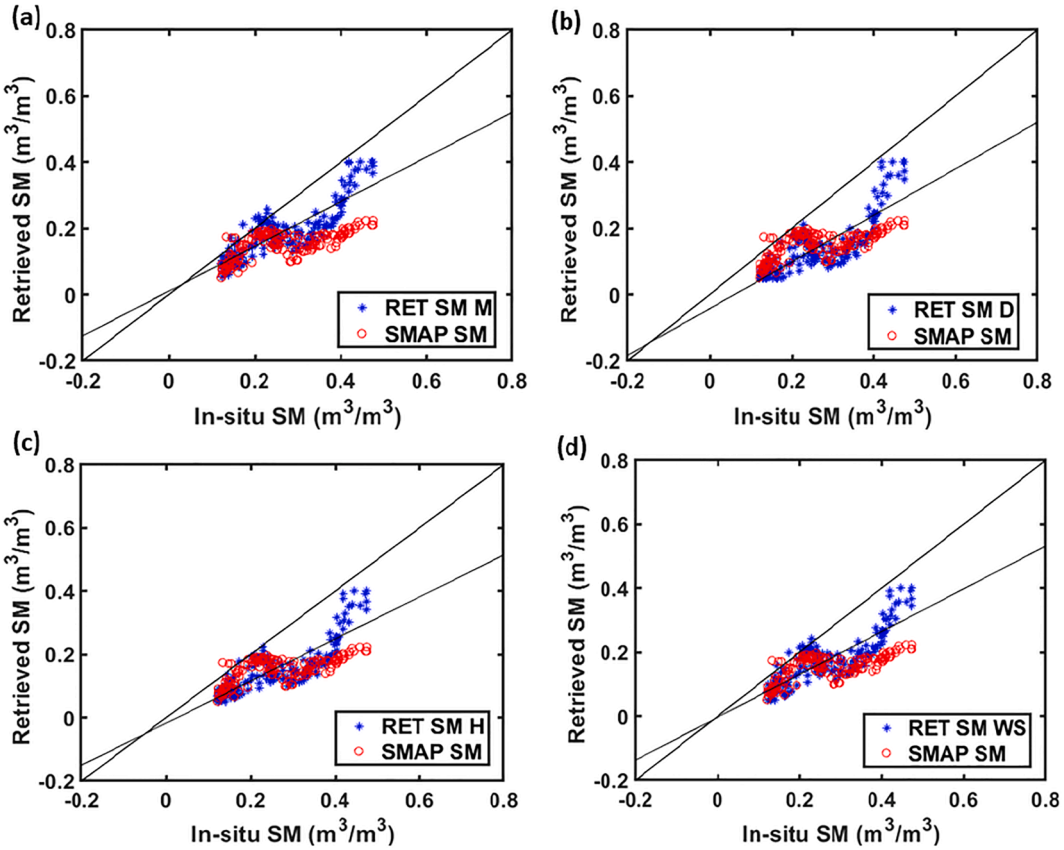

Fig. 15. Scatterplot between In-situ, SMAP SM, GPM rainfall at the Varanasi, UP for (a) RET SM M, (b) RET SM D, (c) RET SM H, (d) RET SM WS.

also performed well but less than the soil dielectric mixing models retrieved SM at the site with RMSE = 0.12, R^2 = 0.53 and PBIAS = −27.90. Scatter plot between the in-situ SM, SMAP SM, retrieved SM using Mironov dielectric model (RET SM M) is presented in Fig. 15(a) along with retrieved SM using Dobson dielectric model (RET SM D) in Fig. 15(b), retrieved SM using Hallikainen dielectric model (RET SM H) in Fig. 15(c), retrieved SM using Wang & Schmugge dielectric model (RET SM WS) in Fig. 15(d). Results of the performance of the dielectric models and SMAP SM is presented in Table 4.

4.3.3. Temporal consistency at the station

For Varanasi, Fig. 16(a) present the temporal series plot between in-situ SM, Mironov retrieved SM (RET SM M), SMAP SM and GPM rainfall and Fig. 16(b) for Dobson model retrieved SM (RET SM D) over Varanasi during June 2017–May 2018. Heavy precipitation can be observed during June–October 2017 and during few days of February and April 2018. At Varanasi, all the retrieved and satellite SM underestimated the ground measured SM estimates, but the SM estimates retrieved using dielectric models performed better the SMAP. However, it's interesting to notice a similar pattern of all the simulated SM variation in natural

Table 4
Results of comparison of different Dielectric Models used in this study at Varanasi, U.P., India.

Statistical test	SMAP SM	Mironov	Dobson	Hallikainen	Wang & Schmugge
Square of Correlation (R^2)	0.53	0.82	0.79	0.79	0.81
RMSE (m^3/m^3)	0.12	0.08	0.11	0.10	0.09
PBIAS	−27.90	−19.60	−29.80	−26.40	−23.20

environmental condition using passive microwave approaches, especially under prevailing climatic extremes. Although, all the dielectric models performed better the SMAP SM, Mironov marginally had better performance than the other models– Dobson model, Hallikainein model, Wang & Schmugge model with better correlation between observed and simulated data set, less bias and lesser RMSE.

Fig. 17(a) presents the temporal plot between in-situ SM, Hallikainen retrieved SM (RET SM H), SMAP SM and GPM rainfall data while Fig. 17 (b) shows plot between in-situ SM, Wang & Schmugge retrieved SM (RET SM WS), SMAP SM and GPM rainfall estimates.

4.4. Performance of Pooled data sets of all the three sites

This sub-section presents the overall performance of the dielectric models selected for this study at all the sites. Results of the statistical tests are summarized in Table 5. Based on RMSE scores for all the dielectric models used in this analysis, the Mironov model (RMSE = 0.07 m^3/m^3) showed best performance than the Wang & Schmugge model (RMSE = 0.08 m^3/m^3), Hallikainen model (RMSE = 0.09 m^3/m^3) and Dobson model (RMSE = 0.10 m^3/m^3) at the validation sites . SMAP radiometer SM product also performed well (RMSE = 0.12 m^3/m^3) at these sites. Also, SM estimates derived using Mironov model showed the highest correlation with the in-situ data set (R^2 = 0.80) followed by the Wang & Schmugge model (R^2 = 0.74), Dobson model (R^2 = 0.72), Hallikainen model (R^2 = 0.67) and SMAP SM (R^2 = 0.57). SMAP SM showed the least bias when compared with ground measured SM (PBIAS = −11.8) at the sites followed by Mironov model (PBIAS = −16.3), Wang model (PBIAS = −18.8), Hallikainen (PBIAS = −21.8) and highest by Dobson model (PBIAS = −32.9) however all the retrieved and satellite SM showed an underestimating pattern for the entire span of this analysis at all the sites.

5. Conclusion

Accurate and efficient retrieval of SM using passive microwave data depends mainly on careful selection of retrieval parameter such as Soil dielectric mixing models, VWC, LST etc. This study provides a detail analysis of the behavior of these parameters and also their role in SM retrieval. Many dielectric mixing models have been reported previously but their practical application was often limited due their complex methodologies, site-specific applicability and lack of continuous in-situ data set to assess their performance. As such this study presents a detailed summary of some of the most widely used dielectric mixing models and present their performances in SM retrieval and reports first of a kind of analysis over Indian agricultural sites. Results of this analysis shows promising performance of Mironov dielectric model in SM retrieval at all selected sites and also exhibit comparatively better performances of all the dielectric models selected in this study than the global SMAP L3 SM product in accurately predicting the surface SM content. This study also highlights limitation and performance of satellite SM product and passive microwave retrieval approaches for widely varying climatic and vegetation condition prevailing in tropical countries like India.

This study underlines the significance of long term in-situ SM data in satellite measurement of surface SM. The ground-based or in-situ SM networks are believed to play an essential role in this study as they are

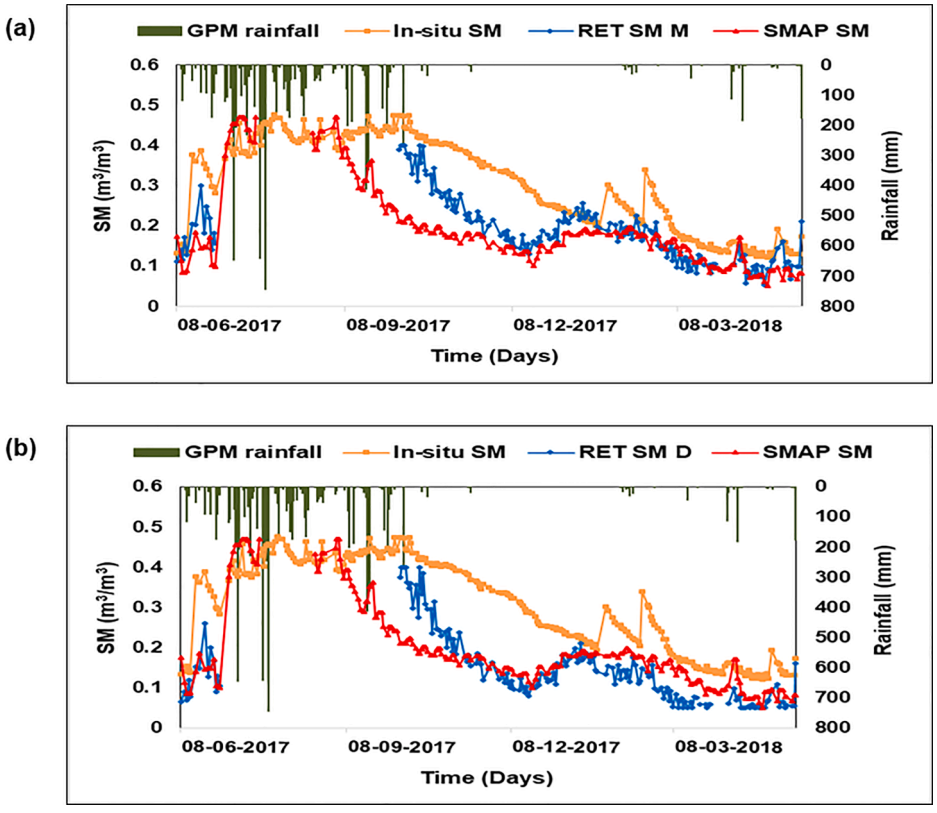

Fig. 16. Scatterplot between In-situ, SMAP SM, GPM rainfall at the Varanasi, UP for (a) RET SM M, (b) RET SM D.

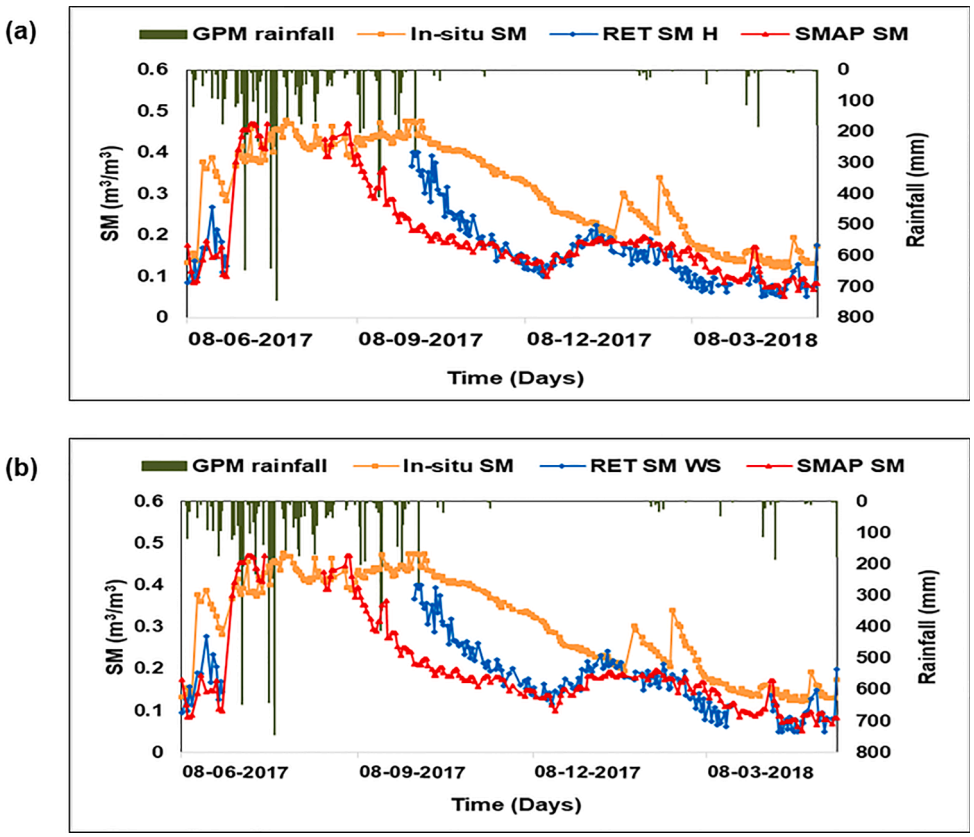

Fig. 17. Scatterplot between In-situ, SMAP SM, GPM rainfall at the Varanasi, UP for (a) RET SM H, (b) RET SM WS.

Table 5
Results of comparison at the selected sites and Pooled performance of different Dielectric Models used in this study.

	Anand, Gujarat			Hoshangabad, M.P.			Varanasi, U.P.			Pooled		
	RMSE (m^3/m^3)	R^2	PBIAS	RMSE (m^3/m^3	R^2	PBIAS	RMSE (m^3/m^3	R^2	PBIAS	RMSE (m^3/m^3	R^2	PBIAS
SMAP	0.09	0.34	43.60	0.13	0.84	−28.10	0.12	0.53	−27.90	0.12	0.57	−11.8
Mironov	0.03	0.68	5.0	0.10	0.70	−18.10	0.08	0.82	−19.60	0.07	0.80	−16.3
Dobson	0.03	0.63	−5.40	0.13	0.76	−26.10	0.11	0.79	−29.80	0.10	0.72	−32.9
Hallikainen	0.04	0.51	12.0	0.11	0.74	−22.50	0.10	0.79	−26.40	0.09	0.67	−21.8
Wang & Schmugge	0.04	0.61	4.80	0.10	0.78	−18.70	0.09	0.81	−23.20	0.08	0.74	−18.80

the mainstay in calibration and validation land surface models and vital in the assessment of the quality of SM products from spaceborne SM missions. Since accurate SM measurements are believed to play a crucial role in minimizing the economic and social losses due to extreme weather events like flood and drought, losses due to crop failures, minimizing wastage of freshwater resources through irrigation scheduling and many more advantages including a better understanding of significant hydrological and environmental processes, this study also recommends framing a roadmap for establishing more dense ground-based SM network, as developed at some of the study sites of this investigation.

In terms of SM retrieval, the MPDI has a lot of potential, especially for sparse or moderate vegetation surface conditions. It is one of the most often used vegetation indicators because of its crucial role in assessing surface structure, moisture content, and roughness in various terrain types. With SM, MPDI increases, while with VWC, it decreases. We noticed a similar pattern of fluctuation in these three parameters at all of our chosen sites. Surface temperature variations can also have a significant impact on MPDI. As a result, this study demonstrates use MPDI to determine the prevailing vegetation conditions for precise SM retrievals.

Although in this study, we used SCA algorithm for the SM retrieval process, more robust and efficient approaches can be developed by testing efficiency of other retrieval algorithms such as dual-channel or Microwave Polarization Ration Algorithm (MPRA) based on Land Parameter Retrieval Model (LPRM) and other dielectric mixing models for better results. Results of this would be useful in developing high performance finer resolution SM product.

CRediT authorship contribution statement

Swati Suman: Data curation, Formal analysis, Investigation, Methodology, Writing - original draft. **Prashant K. Srivastava:** Conceptualization, Data curation, Funding acquisition, Investigation, Methodology, Project administration, Resources, Supervision, Writing - original draft, Writing - review & editing. **Dharmendra K. Pandey:** Data curation, Project administration. **Rajendra Prasad:** Funding acquisition, Writing - original draft, Writing - review & editing. **RK Mall:** Project administration, Writing - review & editing. **Peggy O'Neill:** Project administration, Writing - original draft.

Declaration of Competing Interest

The authors declare that they have no known competing financial

interests or personal relationships that could have appeared to influence the work reported in this paper.

Acknowledgments

Authors wish to thank Space Applications Center (SAC), Indian Space Research Organization (ISRO), India for providing in-situ data and their funding. Also, to all the co-authors for their valuable contribution and suggestions. The authors would also like to express their gratitude to the editor and anonymous reviewers for their constructive comments and feedback in developing this work.

References

Al-Shrafany, D., Rico-Ramirez, M.A., Han, D., 2012. Calibration of roughness parameters using rainfall–runoff water balance for satellite soil Moisture retrieval. J. Hydrol. Eng. 17 (6), 704–714.

Anav, A., Proietti, C., Menut, L., Carnicelli, S., De Marco, A., Paoletti, E., 2018. Sensitivity of stomatal conductance to soil moisture: implications for tropospheric ozone. Atmos. Chem. Phys. 18 (8), 5747–5763.

Anjum, M.N., Ding, Y., Shangguan, D., Ahmad, I., Ijaz, M.W., Farid, H.U., et al., 2018. Performance evaluation of latest integrated multi-satellite retrievals for Global Precipitation Measurement (IMERG) over the northern highlands of Pakistan. Atmos. Res. 205, 134–146.

Carr, N., Kirstetter, P.-E., Hong, Y., Gourley, J., Schwaller, M., Petersen, W., et al., 2015. The influence of surface and precipitation characteristics on TRMM Microwave Imager rainfall retrieval uncertainty. J. Hydrometeorol. 16 (4), 1596–1614.

Chen, D., Tian, Y., Yao, T., Ou, T., 2016. Satellite measurements reveal strong anisotropy in spatial coherence of climate variations over the Tibet Plateau. Sci. Rep. 6 (1), 1–9.

Chen, F., Crow, W.T., Colliander, A., Cosh, M.H., Jackson, T.J., Bindlish, R., Reichle, R. H., Chan, S.K., Bosch, D.D., Starks, P.J., Goodrich, D.C., Seyfried, M.S., 2017. Application of triple collocation in ground-based validation of Soil Moisture Active/Passive (SMAP) level 2 data products. IEEE J Sel. Top. Appl. Earth Obs. Remote Sens. 10 (2), 489–502.

Cole, K.S., Cole, R.H., 1941. Dispersion and absorption in dielectrics I. Alternating current characteristics. J. Chem. Phys. 9 (4), 341–351.

Colliander, A., Cosh, M.H., Misra, S., Jackson, T.J., Crow, W.T., Chan, S., Bindlish, R., Chae, C., Holifield Collins, C., Yueh, S.H., 2017. Validation and scaling of soil moisture in a semi-arid environment: SMAP validation experiment 2015 (SMAPVEX15). Remote Sens. Environ. 196, 101–112.

Cosh, M.H., Ochsner, T.E., McKee, L., Dong, J., Basara, J.B., Evett, S.R., Hatch, C.E., Small, E.E., Steele-Dunne, S.C., Zreda, M., Sayde, C., 2016. The soil moisture active passive Marena, Oklahoma, in-situ sensor testbed (smap-moisst): Testbed design and evaluation of in-situ sensors. Vadose Zo. J. 15 (4), 1–11.

Curtis, J.O., 2001. Moisture effects on the dielectric properties of soils. IEEE Trans. Geosci. Remote Sens. 39 (1), 125–128.

Debye, P.J.W., 1929. Polar Molecules. Chemical Catalog Company Incorporated.

Dobson, M., Ulaby, F., Hallikainen, M., El-rayes, M., 1985. Microwave dielectric behavior of wet soil-Part II: dielectric mixing models. IEEE Trans. Geosci. Remote Sens. 35–46.

Felde, G.W., 1998. The effect of soil moisture on the 37GHz microwave polarization difference index (MPDI). Int. J. Remote Sens. 19 (6), 1055–1078.

Hallikainen, M., Ulaby, F., Dobson, M., El-rayes, M., Wu, L.-K., 1985. Microwave dielectric behavior of wet soil-part 1: empirical models and experimental observations. IEEE Trans. Geosci. Remote Sens. GE-23 (1), 25–34.

Heimovaara, T.J., Bouten, W., Verstraten, J.M., 1994. Frequency domain analysis of time domain reflectometry waveforms: 2. A four-component complex dielectric mixing model for soils. Water Resour. Res. 30 (2), 201–209.

Jackson, T.J., 1993. III. Measuring surface soil moisture using passive microwave remote sensing. Hydrol. Process. https://doi.org/10.1002/hyp.3360070205.

Jackson, T.J., Hsu, A.Y., O'Neill, P.E., 2002. Surface soil moisture retrieval and mapping using high-frequency microwave satellite observations in the Southern Great Plains. J. Hydrometeorol. 3 (6), 688–699.

Jackson, T.J., Hurkmans, R., Hsu, A., Cosh, M.H., 2004. Soil moisture algorithm validation using data from the Advanced Microwave Scanning Radiometer (AMSR-E) in Mongolia.

Jackson, T.J., Schmugge, T.J., 1991. Vegetation effects on the microwave emission of soils.

Knoll, M.D., Knight, R., 1994. Relationships between dielectric and hydrogeologic properties of sand–clay mixtures. Fifth International Conference on Ground Penetrating Radar 45–61.

Loor, G.P.d., 1968. Dielectric properties of heterogeneous mixtures containing water. J. Microw. Power 3 (2), 67–73.

Ma, L.u., Zhao, L., Tian, L.-M., Yuan, L.-M., Xiao, Y., Zhang, L.-l., Zou, D.-f., Qiao, Y.-P., 2019. Evaluation of the integrated multi-satellite retrievals for global precipitation measurement over the Tibetan Plateau. J. Mount. Sci. 16 (7), 1500–1514.

Mironov, V.L., Dobson, M.C., Kaupp, V.H., Komarov, S.A., Kleshchenko, V.N., 2004. Generalized refractive mixing dielectric model for moist soils. IEEE Trans. Geosci. Remote Sens. 42 (4), 773–785.

Mladenova, I., Lakshmi, V., Jackson, T.J., Walker, J.P., Merlin, O., de Jeu, R.A.M., 2011. Validation of AMSR-E soil moisture using L-band airborne radiometer data from National Airborne Field Experiment 2006. Remote Sens. Environ. https://doi.org/10.1016/j.rse.2011.04.011.

Mladenova, I.E., Jackson, T.J., Njoku, E., Bindlish, R., Chan, S., Cosh, M.H., Holmes, T.R. H., de Jeu, R.A.M., Jones, L., Kimball, J., Paloscia, S., Santi, E., 2014. Remote monitoring of soil moisture using passive microwave-based techniques—theoretical basis and overview of selected algorithms for AMSR-E. Remote Sens. Environ. 144, 197–213.

Montzka, C., Cosh, M., Bayat, B., Al Bitar, A., Berg, A., Bindlish, R., et al., 2020. Soil Moisture Product Validation Good Practices Protocol Version 1.0. Good Practices for Satellite Derived Land Product Validation, pp. 123.

Nguyen, B., Geels, A.M., Bruining, J., Slob, E.C., 1997. Calibration measurements of dielectric properties of porous media. SPE Journal 4, 353–359.

Srivastava, P.K., O'Neill, P., Cosh, M., Kurum, M., Lang, R., Joseph, A., 2014. Evaluation of dielectric mixing models for passive microwave soil moisture retrieval using data from ComRAD ground-based SMAP simulator. IEEE J Sel. Top. Appl. Earth Obs. Remote Sens. 8 (9), 4345–4354.

Van Dam, R.L., 2014. Calibration functions for estimating soil moisture from GPR dielectric constant measurements. Commun. Soil Sci. Plant Anal. 45 (3), 392–413.

Van Dam, R.L., Borchers, B., Hendrickx, J.M.H., 2005. Methods for prediction of soil dielectric properties: a review. In: Detection and Remediation Technologies for Mines and Minelike Targets X. International Society for Optics and Photonics, pp. 188–197.

Wang, J.R., Schmugge, T.J., 1980. An empirical model for the complex dielectric permittivity of soils as a function of water content. IEEE Trans. Geosci. Remote Sens. 288–295.

Wensink, W.A., 1993. Dielectric properties of wet soils in the frequency range 1–3000 MHz. Geophysical Prospecting 41, 671–696.

Wu, C.-C., Margulis, S.A., 2013. Real-time soil moisture and salinity profile estimation using assimilation of embedded sensor datastreams. Vadose Zone J. 12 (1), 1–17.